Valence Delocalization and Crystal Structure of $[Fe_3O(pazo)_6(py)_3]\cdot 3py$: An Example of the Mixed Valence Delocalization between Two Iron Atoms

Masaaki Manago, Shinya Hayami,† Yayoi Yano, Katuya Inoue,† Risa Nakata, Akiko Ishida, and Yonezo Maeda*

Department of Chemistry and Physics of Condensed Matter, Graduate School of Sciences, Kyushu University, Hakozaki 6-10-1, Higashi-ku, Fukuoka 812-8581

†Institute for Molecular Science, Myodaiji, Okazaki 444-8585

(Received April 22, 1999)

The oxo-centered, trinuclear, mixed-valence complex $[Fe_3O(pazo)_6(py)_3]\cdot 3py$, where pazo is 4-phenylazobenzoic acid, has been prepared, and the intramolecular electron transfer properties in the solid state have been studied. There are two doublets in the area ratio of two (Fe^{3+}) and one (Fe^{2+}) at 78 K. Increasing the sample temperature above 120 K turns these to two doublets in the area ratio of two ($Fe^{2.5+}$) and one (Fe^{3+}); the average valence state between an iron(II) and one of two irons(III) is observed. The complex crystallizes in the C-centered monoclinic space group *C2/c* with 4 molecules in a unit cell which has dimensions: a = 15.856(4), b = 28.649(2), c = 25.739(2) Å, V = 11317(3) Å^3, β = 104.54(1) at 150 K, and a = 15.867(3), b = 28.555(3), c = 25.747(5) Å, V = 11288(3) Å^3, β = 104.60(2) at 85 K. The metal sites of the average valence state and Fe^{3+} state are seen in its single-crystal X-ray structure at both temperatures. The X-ray structure work shows that the dimensions of the Fe_3O triangle become larger and the length of *b*-axis becomes longer with increasing of temperature. There is a C_2 axis in the molecule, Fe_B^{3+} and a pyridine coordinating to the Fe_B^{3+} being located on the axis. The plane of the pyridine is almost perpendicular to that of the Fe_3O triangle and those of other two pyridines coordinating to $Fe^{2.5+}$ ($Fe^{2+}+Fe_A^{3+}$) are parallel to that of the Fe_3O triangle.

Mixed-valence trinuclear iron carboxylate complexes, $[Fe_2^{3+}Fe^{2+}O(O_2CR)_6L_3]\cdot Sol$, are one of the suitable systems for studying mixed-valence properties of molecules in the solid state[1] as well as mixed-valence dinuclear complexes[2] and diferrocene complexes.[3] The first report of ^{57}Fe Mössbauer spectra of the mixed-valence acetate complex $[Fe_3O(O_2CCH_3)_6(H_2O)_3]\cdot nH_2O$ showed a temperature dependent valence-delocalizing process from the localized-valence state at lower temperatures to the delocalized-valence state at room temperature.[4] Many kinds of Fe_3O complexes have been prepared: the complexes with long chain acid anions,[5a] with 1,4,7-triazacyclononane,[5b] and with cyanoacetic acid.[5c] There is a report which gives inelastic neutron scattering reports.[6] Hendrickson et al. have reported many mixed-valence acetate complexes $[Fe_3O(O_2CCH_3)_6L_3]\cdot Sol$.[7] They have shown that the valence-delocalization process occurs as an order-disorder phase transition,[8] and that the rate of intramolecular electron transfer depends on the surrounding environment. The rate of intramolecular electron transfer is sensitively affected by the nature of the coordinated ligands L, and/or solvate molecules Sol. Sato et al. very recently have reported the first example of mixed-valence trinuclear iron carboxylate complexes in which valence delocalizing only between two iron atoms is observed.[9]

The mixed-valence trinuclear complex $[Fe_3O(pazo)_6(py)_3]\cdot 3py$ was prepared, and the valence delocalizing between Fe^{2+} and one of two Fe^{3+} in the Fe_3O complexes was examined with the Mössbauer spectra and single crystal X-ray structure.

Experimental

Preparation of $[Fe_3O(pazo)_6(py)_3]\cdot 3py$. 4-Phenylazobenzoic acid (2.28 g, 10.08 mmol) was dissolved in 30 ml of pyridine, and the solution was stirred for 30 min with bubbling of a constant stream of nitrogen. To this solution $[Fe_3O(O_2CCH_3)_6(H_2O)_3]$ (0.2 g, 0.34 mmol) was dissolved and the reaction mixture was heated at 50—60 °C under nitrogen atmosphere for 1 h with stirring. The mixture was cooled to room temperature and the solvent was evaporated slowly in the stream of nitrogen. After a few days, the single-crystal samples of the complex were separated from other solids. The desolvated complex was obtained by drying of the above complex in vacuum for few days.

Physical Measurements. Mössbauer spectra were measured with an S-600 constant-acceleration spectrometer (Austin Science Associates). Temperature was controlled with a temperature controller, type ITC502 (Oxford Instruments) within a variable temperature cryostat, type DN1726 (Oxford Instruments). The data were stored in a 1024-channel analyzer, type IT-5200 (Inotech Inc.). A 10 mCi cobalt-57 source diffused into palladium foil was used. The spectra were fitted by a Lorentzian line shape using software of

IGOR Pro (Wave Metrics, Inc.) on a personal computer. The velocity scales and isomer shifts were normalized to iron foil at room temperature.

Each reflectance spectrum was measured using a Shimadzu UV-3100PC self-recording spectrophotometer in region from 250 to 800 nm at room temperature.

Crystal Structure. X-Ray structure determinations of the complex were carried out at 293, 150, and 85 K. A brown prismatic single crystal (0.2×0.2×0.2 mm) of the complex was mounted on a glass fiber. All measurements were made on a Rigaku RAXIS II imaging plate area detector with graphite monochromated Mo $K\alpha$ radiation. The structure at 293 K was not solved with reasonable confidence because of the severe disorder of solvent molecules and therefore the data are not discussed here.

Cell constants and an orientation matrix for data collection corresponded to a C-centered ($C2/c$) monoclinic cell with dimensions: a = 15.856(4), b = 28.649(2), c = 25.739(2) Å, V = 11317(3) Å^3, β = 104.54(1) at 150 K, and a = 15.867(3), b = 28.555(3), c = 25.747(5) Å, V = 11288(3) Å^3, β = 104.60(2) at 85 K. For Z = 4 and F.W. = 2246.81, the calculated density is 1.32 g cm^{-3}.

The numbers of measured reflections were 9018 at 150 K, and 9379 at 85 K, respectively. The liner absorption coefficient μ for Mo $K\alpha$ radiation is 4.5 cm^{-1}. The data were corrected for Lorentz and polarization effects. The structure was solved by direct methods and expanded using Fourier techniques. The non-hydrogen atoms were refined anisotropically. Hydrogen atoms were included but not refined. The final cycle of full matrix least-squares refinement at 150 K was based on 6918 observed reflections ($I > 3.00\sigma(I)$) and 723 variable parameters and converged (largest parameter shift was 0.14 times its esd) with unweighted and weighted agreement factors of R = 0.076, R_w = 0.090. At 85 K, the final refinement was carried out with 6254 observed reflections ($I > 3.00\sigma(I)$) and 723 variable parameters and converged (largest parameter shift was 0.19 times its esd) with R = 0.055, R_w = 0.062.

The goodness of fit indicator were 3.09 at 150 K, and 1.43 at 85 K. The weighting scheme was based on counting statistics and included a factor (p = 0.010) to downweight the intense reflections. Plots of $\sum\omega\,(|F_o| - |F_c|)^2$ versus $|F_o|$, reflection order in data collection, $\sin\theta/\lambda$ and various classes of indices showed no unusual trends. The maximum and minimum peaks on the final difference Fourier map corresponded to 0.61 and −1.06 e Å^{-3} at 150 K, and 0.55 and −0.54 e Å^{-3} at 85 K, respectively. (Crystallographic data have been deposited at the CCDC, 12 Union Road, Cambridge CB2 1EZ UK and copies can be obtained on request, free of charge, by quoting the publication citation and the deposition numbers CCDC 130860 and CCDC 130861). The complete $F_o - F_c$ date are deposited as Document No. 72034 at the Office of the Editor of Bull. Chem. Soc. Jpn.

Results and Discussion

Mössbauer Spectra. Mössbauer spectra of the complex were measured at various temperatures and are shown in Fig. 1 with the Lorentzian-line fitted spectra. The spectrum at 78 K shows two doublets, suggesting localized electronic states on the Mössbauer time scale. The doublet with the strong absorption is assigned to the high-spin ($Fe_A^{3+} + Fe_B^{3+}$) and the doublet with the different line widths and intensities is assigned to the high-spin Fe^{2+}. Their absorption areas of Fe^{3+} and Fe^{2+} are seen in an area ratio of 2.06 : 1, which is close to the theoretical ratio of 2 : 1. The values of isomers shift of δ = 0.59 mm s^{-1} and quadrupole splitting of ΔE = 0.93

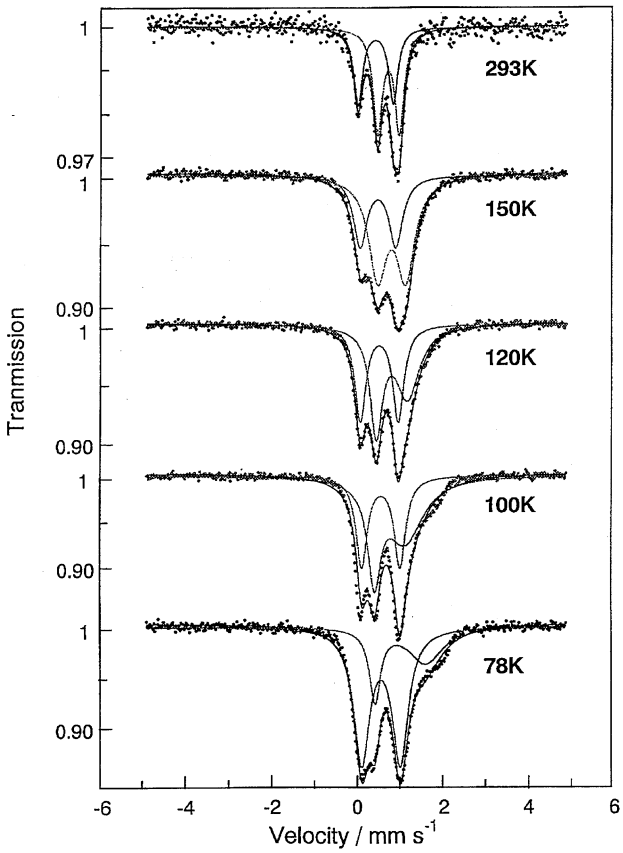

Fig. 1. Temperature dependence of the Mössbauer spectra for the complex.

mm s^{-1} observed for Fe^{3+} are close to the reported ones for Fe^{3+} of $[Fe_3O(O_2CCH_3)_6(3\text{-Mepy})_3]\cdot Sol$,[8b] δ = 0.545 mm s^{-1} and ΔE = 1.045 mm s^{-1}, respectively. The isomer shift of 1.06 mm s^{-1} observed for Fe^{2+} is a little smaller than that observed for Fe^{2+} in octahedral sites and the line width of the high-energy peak is broad. The line broadening is also observed for the spectrum at 100 K. Therefore, it is assumed that the electronic transfer rate between Fe^{2+} and Fe^{3+} is in the order of a little slower than 10^7 s^{-1} between 100 and 78 K, although the spectrum at 78 K shows localized ones. The sample prepared separately showed a little higher transition temperature and a spectrum with the parameters of δ = 1.16 mm s^{-1} and ΔE = 1.53 mm s^{-1} for Fe^{2+} at 95 K (unpublished data).

The spectrum at 293 K is analyzed with two doublets of Fe^{3+} and $Fe^{2.5+}$. The doublet of δ = 0.75 mm s^{-1} is assigned to the delocalized valence state $Fe^{2.5+}$ ($Fe^{2+} + Fe_A^{3+}$) and that of δ = 0.44 mm s^{-1} to Fe_B^{3+}, of which absorptions are observed in the area ratio of 1.86 : 1. Least-squares fitting of the spectra to Lorentzian line shapes (solid lines) clearly indicates that the spectrum is comprised of only two doublets. The Mössbauer fitting parameters are summarized in Table 1. As the temperature is increased, the absorption of Fe_{mix} (the components which constitute $Fe^{2.5+}$ are temporally named here) gains peak intensity with the expense of the absorption of Fe^{3+}, and the isomer shift of the Fe_{mix} doublet decreases from 1.06 mm s^{-1} at 78 K to 0.75 mm s^{-1}

Table 1. Mössbauer Parameters for the Complex and the Desolvated Complex

Complex	δ/mm s^{-1}		ΔE_Q/mm s^{-1}		Γ/mm s^{-1}			Area/%		$\sum\chi^2(\times10^{-3})$[d]
	T/K	Fe^{II}	Fe^{III}	Fe^{II}	Fe^{III}	Fe^{II} Γ_l[b]	Fe^{II} Γ_h[c]	Fe^{III}	Fe^{II}	Fe^{III}	
Solvated complexes	78	1.06	0.59	1.21	0.93	0.32	1.00	0.46	32.63	67.37	5.98
	T/K	Fe_{mix}[a]	Fe^{III}_B	Fe_{mix}[a]	Fe^{III}_B	Fe_{mix}[a] Γ_l[b]	Fe_{mix}[a] Γ_h[c]	Fe^{III}_B	Fe_{mix}[a]	Fe^{III}_B	
	100	0.80	0.59	0.74	0.92	0.38	0.90	0.33	60.96	39.04	13.2
	120	0.85	0.54	0.75	0.91	0.36	0.68	0.33	58.06	41.94	2.95
	150	0.84	0.51	0.67	0.86	0.53		0.40	64.93	35.07	2.16
	293	0.75	0.44	0.52	0.85	0.28	0.29	0.26	64.98	35.02	0.90
	T/K	Fe^{II}	Fe^{III}	Fe^{II}	Fe^{III}	Fe^{II}		Fe^{III}	Fe^{II}	Fe^{III}	
Desolvated complexes	95	1.30	0.56	1.92	1.06	0.56		0.36	34.48	65.52	5.52
	200	1.23	0.53	1.25	0.92	0.46		0.33	32.31	67.69	2.01
	293	1.06	0.50	0.93	0.87	0.46		0.34	34.22	65.78	1.95

a) Components which constitute $Fe^{2.5+}$ valence-state at high temperature ($Fe^{II}+Fe^{III}_A$). b) Full width at half-maximum of the low energy component of the doublet. c) Full width at half-maximum of the high energy component of the doublet. d) Residual sum.

at 293 K. The value of the doublet is not characteristic of that of high-spin Fe^{2+} any longer, but is in agreement with the reported values of 0.7—0.8 mm s^{-1} for the averaged valence state.[2c] No component of the Fe^{3+} doublet or the Fe_{mix} doublet exhibits any line broadening at 293 K and the quadrupole splitting of Fe_{mix} at 293 K is smaller than those of Fe^{2+} and Fe^{3+} at 78 K; similar examples have been observed for $[Fe_3O(O_2CCH_2CN)_6(H_2O)_3]$.[5c] This result suggests that the temperature dependence of the quadrupole splitting of "Fe^{2+}" is very large and/or the signs of the electric field gradient of "Fe^{2+}" and Fe^{3+}_A are opposite each other. There are three solvent molecules in the Fe_3O unit, different from the complexes reported until now. An example of the relaxation between electric states with the opposite signs in electric field gradient is reported for the spin-crossover complexes,[10] the minimum value of quadrupole splitting being observed in the transition temperature range from the low-spin to high-spin state in the case, in which the signs of the electric field gradient of the high-spin and the low-spin states are inverse to each other.

The spectrum at 100 K is complex and the same assignment as that at 120 K does not bring about a good fitting. Especially the shoulder observed at 2 mm s^{-1} is not fitted reasonably, and the Mössbauer parameters obtained by the simulation with two doublets are not in systematic change, suggesting that the spectrum shows relaxation between Fe^{2+} and Fe^{3+}. The rate of intramolecular electron transfer between Fe^{2+} and Fe^{3+} atoms in the Fe_3O moiety is slower than the inverse of the Mössbauer time scale of 10^{-7} s below 78 K, increases to the time scale with increasing temperature between 78 and 100 K, and exceeds the time scale above 120 K. The temperature dependences of the isomer shifts and quadrupole splittings are shown in Figs. 2 and 3, respectively. The large spectral change observed between 78 and 100 K is in accordance with the change in the valence state from the localized to the delocalized state. The temperature dependence of the isomer shifts is reasonable above 120 K,

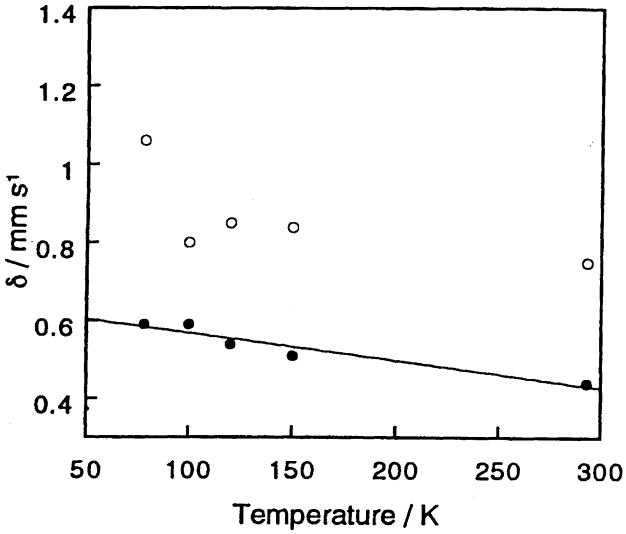

Fig. 2. Temperature dependence of the isomer shifts for the complex. (●) for Fe^{3+} and (○) for Fe_{mix} (or Fe^{2+}).

being in accord with a second order Doppler shift.

Desolvated complexes were prepared by keeping the complexes in vacuum for several days, after which the Mössbauer spectra were measured. The spectra show localized spectra as shown in Fig. 4 and the quadrupole splittings assigned to Fe^{2+} show strong temperature dependence. Existence of solvent molecules may have some effect on the rate of electron transfer between Fe^{2+} and Fe^{3+}.

Reflectance Spectrum. The reflectance spectrum of the complex was measured at room temperature and is deposited in the editorial office (Fig. S-1). The sharp band at 320 nm is assigned to 4-phenylazobenzoic acid and the broad band which may be assigned to an intervalence-transfer band is observed at 580 nm, but the lack of the resolution precludes detailed analysis.

Single-Crystal X-Ray Structure of the Trinuclear Complexes at 150 and 85 K. The atomic parameters of the

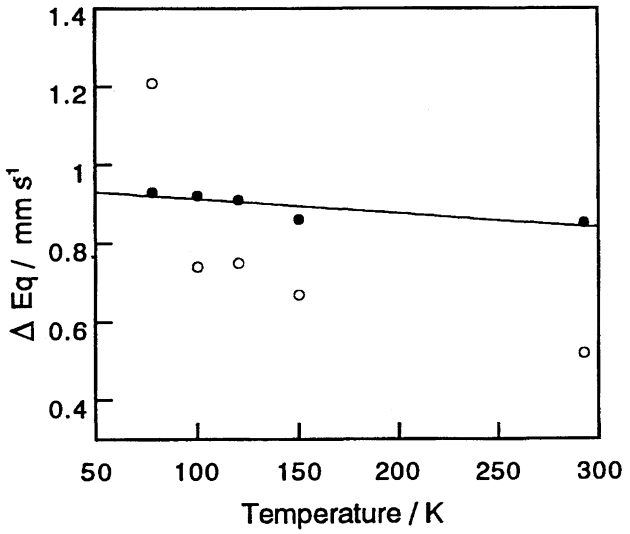

Fig. 3. Temperature dependence of the quadrupole splitting for the complex. (●) for Fe^{3+} and (○) for Fe_{mix} (or Fe^{2+}).

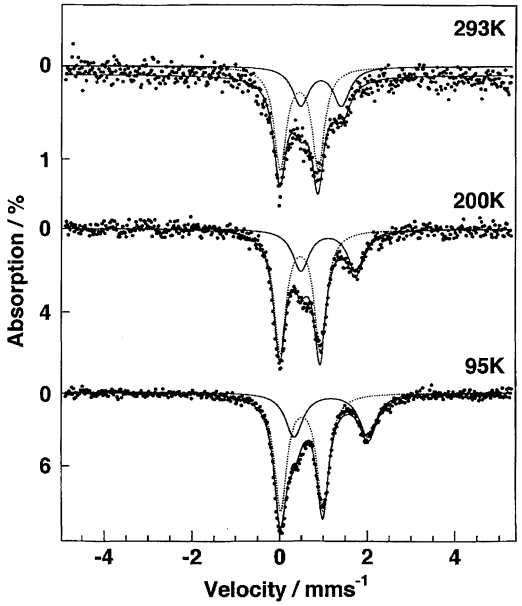

Fig. 4. Mössbauer spectra of the desolvated complex at 293, 200, and 95 K.

Table 2. Representative Bond Lengths and Angles for the Complex at 85 and 150 K

	Bond lengths (Å)	
	85 K	150 K
Fe(1)–O(1)	1.836(4)	1.851(6)
Fe(1)–O(2)	2.052(3)	1.990(4)
Fe(1)–O(7)	2.000(3)	2.061(4)
Fe(1)–N(1)	2.256(5)	2.250(8)
Fe(2)–O(1)	1.935(2)	1.934(3)
Fe(2)–O(3)	2.071(3)	2.107(4)
Fe(2)–O(4)	2.103(3)	2.064(4)
Fe(2)–O(5)	2.067(3)	2.102(4)
Fe(2)–O(6)	2.097(3)	2.069(4)
Fe(2)–N(2)	2.213(4)	2.207(5)
Fe(1)–O_{av}	1.988	1.991
Fe(2)–O_{av}	2.055	2.056
	Bond angles (°)	
O(1)–Fe(1)–O(2)	93.41(8)	99.9(1)
O(1)–Fe(1)–O(7)	99.81(8)	93.4(1)
O(1)–Fe(1)–N(1)	180.0000(1)	180.0000(1)
O(2)–Fe(1)–O(2)	173.2(2)	160.3(3)
O(2)–Fe(1)–O(7)	99.81(8)	93.1(2)
O(2)–Fe(1)–N(1)	86.59(8)	80.1(1)
O(2)–Fe(1)–O(7)	86.0(1)	85.7(2)
O(2)–Fe(1)–O(7)	92.8(1)	93.1(2)
O(2)–Fe(1)–N(1)	86.59(8)	80.1(1)
O(7)–Fe(1)–O(7)*	160.4(2)	173.2(3)
O(7)–Fe(1)–N(1)	90.19(8)	86.6(1)
O(1)–Fe(2)–O(3)	91.5(1)	98.6(2)
O(1)–Fe(2)–O(4)	95.0(1)	95.5(2)
O(1)–Fe(2)–O(5)	95.7(1)	95.0(2)
O(1)–Fe(2)–O(6)	98.7(1)	91.3(2)
O(1)–Fe(2)–N(2)	176.1(1)	176.4(1)
O(3)–Fe(2)–O(4)	92.2(1)	87.8(2)
O(3)–Fe(2)–O(5)	172.8(1)	165.7(2)
O(3)–Fe(2)–O(6)	92.4(1)	91.6(2)
O(3)–Fe(2)–N(2)	84.8(1)	82.8(2)
O(4)–Fe(2)–O(5)	86.3(1)	86.5(2)
O(4)–Fe(2)–O(6)	165.4(1)	173.2(2)
O(4)–Fe(2)–N(2)	83.9(1)	87.9(2)
O(5)–Fe(2)–O(6)	87.4(1)	92.5(2)
O(5)–Fe(2)–N(2)	88.0(1)	83.9(2)
O(6)–Fe(2)–N(2)	82.7(1)	85.3(2)
Fe(1)–O(1)–Fe(2)	120.00(1)	119.9(2)
Fe(2)–O(1)–Fe(2)*	120.0(2)	120.2(3)

complex at 85 and 150 K are deposited in the editorial office (Table S-1). The selected bond lengths and angles for the central atoms of the Fe_3O triangle are collected in Table 2. An ORTEP drawing of the molecular structure at 150 K with its atom-labeling scheme is given in Fig. 5. The Fe_3O moiety has a typical triangular unit, where three iron atoms are bridged with the center oxygen atom and the six carboxylates, and a pyridine ligand coordinates to each iron atom.

In the analogous acetate compound, the molecules are located on sites with crystallographic 3-fold symmetry, so that the three iron atoms are indistinguishable,[7a,7d] and this is attributed to dynamic disordering resulting from rapid intramolecular electron transfer. On the other hand, the molecule of this complex has a 2-fold symmetry axis in the molecule; the Fe(1) atom located on the C_2 axis is in the high-spin Fe^{3+} state (Fe_B^{3+}) from the comparison of the bond lengths between each iron atom and the coordinating oxygen atoms. The Fe(1)–$O(1)_{oxide}$ and Fe(2)–$O(1)_{oxide}$ distances are 1.851(6) and 1.934(3) Å at 150 K, respectively, and the average Fe(1)–$O_{carboxylate}$ distance is 2.025 Å, which is ca. 0.044 Å shorter than the average Fe(2)–$O_{carboxylate}$ (2.069 Å). The values of Fe(1)–O are close to the typical values for iron(III)–oxygen, and those of Fe(2)–O are intermediate between the typical Fe(III)–O and Fe(II)–O distance.[11] These results are in good agreement with the observation that the Mössbauer spectra indicate that one of the three iron atoms in the Fe_3O moiety is in a trivalent state and the others are a 2.5 valence state. The other bond distances

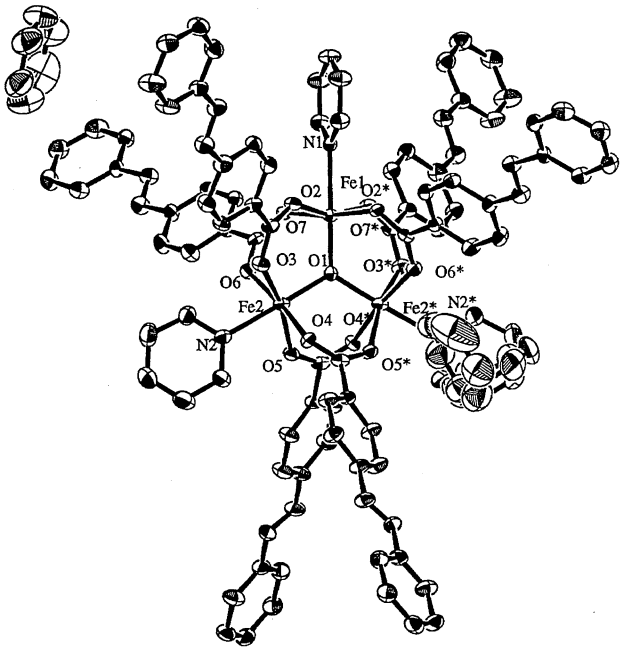

Fig. 5. ORTEP plot of the molecular structure of the complex at 150 K.

about the iron atoms show an interesting anomaly. The distances to the central oxygen are one short and two long, but iron-nitrogen distances are the other way round; Fe1–N(1), 2.250(8); Fe2–N(2), 2.207(5) Å. This type of inversion has been observed in another oxo-centered mixed-valence complex, $[Fe_3O(O_2CCMe_3)_6(py)_3]$.[12]

There is no change in the space group in the temperature range from 85 to 298 K. The structure at 85 K was the almost same as that at 150 K. The length of the *b* axis at 85 K is shorter than that at 150 K, and the lengths of the *a* and *c* axes are longer than the corresponding ones at 150 K. The length of Fe–O(1) becomes short and those of Fe–N become long with decreasing of temperature. The bond lengths of Fe(1)–O_{av} and Fe(2)–O_{av} become short with decreasing of temperature. At first sight it seems strange that the two iron atoms Fe(2) and Fe(2)* are crystallographically equivalent at 85 K, although the Mössbauer spectrum indicates localized Fe^{2+} and Fe^{3+} at 78 K. This inconsistency can be explained by the following consideration of the time needed for observing resonance absorption: The average electronic state in 10^{-7} s is observed on the Mössbauer spectra. The information from X-ray diffraction patterns contains averaged molecular structure over the long range (about 500 nm) of a crystal. Although the localized valence states are observed in the Mössbauer spectrum at 78 K, it does not imply that the valence states are delocalized on a time scale longer than 10^{-6} s. A similar phenomenon has been reported for $[Fe_2(bpmp)(ena)](BF_4)_2$ (bpmp = 2, 6-bis[bis(2-pyridylmethyl)aminomethyl]-4-methylphenol and ena = $O_2C(CH_2)_6CH_3$).[13]

In the Fe_3O moiety, the planes of two of the three pyridine ligands (pyridine A) coordinating to the Fe atoms are almost parallel to the Fe_3O plane (8.77°), while the last pyridine ligand (pyridine B) is nearly perpendicular to the Fe_3O plane (89.10°). The dihedral angle of the plane of pyridines A and B is 81.19°; this value is close to 82.8° for $[Fe_3O(O_2CCH_3)_3(3\text{-Mepy})_3](CH_3CN)$.[11b] Hendrickson et al. have reported four types of mixed-valence Fe_3O moiety having 3, 2, 1, or 0 pyridine or substituted pyridine ligands in the Fe_3O plane. They suggested that the conformation of the (substituted) pyridine ligands is one of the major factors determining whether a Fe_3O moiety is valence localized or delocalized.[8b] The Fe–O distances observed for asymmetric types, provide further evidence that the orientations of pyridine ligands influence the charge distribution. It should be noted that, in the case of asymmetric types, the "extra electron" resides primarily on the iron atoms with pyridine ligands in the Fe_3O plane.[8c] Actually, in the case of $[Fe_3O(O_2CCH_3)(4\text{-Etpy})_3]\cdot(4\text{-Etpy})$, the planes of the two 4-Etpy ligands bonded to the two Fe^{3+} atoms are perpendicular to the Fe_3O plane, and the plane of the third 4-Etpy ligand is parallel to that by single-crystal X ray structure.[8c] An iron atom coordinated with the in-plane 4-ethylpyridine ligand is easily assigned to a ferrous one from the comparison of the bond lengths for each iron atom. In $[Fe_3O(pazo)(py)_3]\cdot 3py$, the planes of the two pyridine bonded to the two Fe atoms are parallel to the Fe_3O plane. Therefore an extra electron is shared with two symmetrically sited Fe atoms with these planes.

Another important factor controlling whether a Fe_3O moiety is valence localized or delocalized is the existence of solvate molecules. Most of the analogous oxo-centered trinuclear compounds crystallize with extra solvent molecules. The mixed valence state is depending on the presence or absence of solvate molecules. Although pyridine-solvated acetate complex $[Fe_3O(O_2CCH_3)(py)_3]py$ and the nonsolvated complex $[Fe_3O(O_2CCH_3)(py)_3]$ both show a valence-localized state at lower temperature in ^{57}Fe Mössbauer spectroscopy, the solvated complex becomes valence-delocalized at about 190 K, whereas the nonsolvated complex remains in the valence-localized state even at 315 K.[8c] The calorimetric study[14] and ^2H NMR study[7a] have demonstrated that the valence-delocalizing process in the pyridine-solvated complex crystals occurs as an order–disorder phase transition accompanied by orientational disordering of the pyridine solvate molecules. The interaction between the molecular dipole of the electron-localized Fe_3O complex and the permanent dipole moment of the solvate molecule has been considered to play an important role. In the present complex, a strong efflorescence is observed, which indicates that a number of solvate molecules are weakly bonded in the crystal of the complex. It is exhibited by X-ray crystallography that three solvated pyridine molecules are involved in the complex. The packing arrangement of the complex in the *bc*-plane is illustrated in Fig. 6. A cavity made by the Fe_3O moiety and ligand pazo is seen in the plane where pyridine molecules are located. The distributions of pyridine molecules around Fe^{2+} and Fe_A^{3+} are equivalent to each other. Fe_B^{3+} is geometrically surrounded by more solvent pyridines than Fe^{2+} and Fe_A^{3+}, and therefore the site of Fe_B^{3+} may prefer +3 valence state.

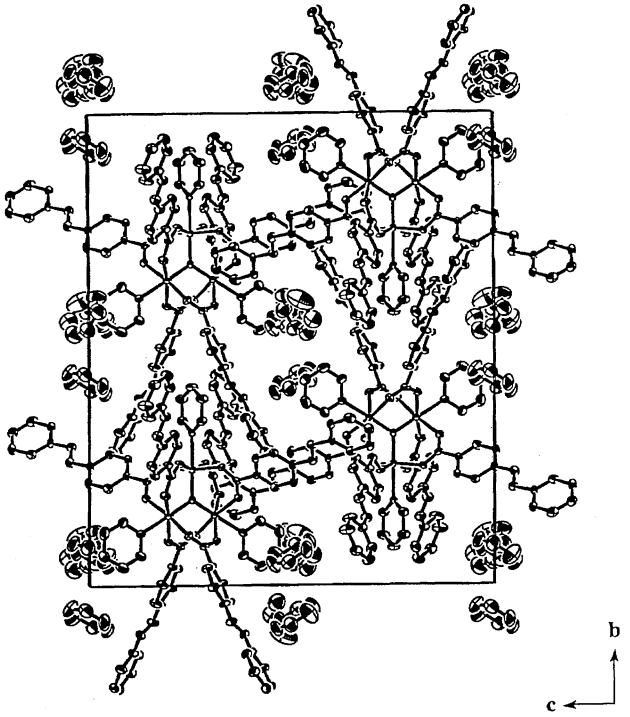

Fig. 6. Packing arrangement of the complex in *bc*-plane.

However, it has been found that some nonsolvated mixed-valence Fe_3O complexes, such as $[Fe_3O(O_2CC_{17}H_{35})_6(py)_3]$,[5a,15] which have long alkyl groups, also show a valence-delocalizing phase transition below room temperature. These results have indicated that the valence-delocalizing phase transition is not always related to the presence of solvent molecules, and they suggest that the substituents of carboxylated ligands may play an important role in place of the solvate molecules.

A Grant-in Aid for Scientific Research No. 10149238 from the Ministry of Education, Science, Sports and Culture is greatly acknowledged.

References

1 C. T. Dziobkowski, J. T. Wrobleski, and D. B. Brown, *Inorg. Chem.*, **20**, 679 (1981).

2 a) M. Suzuki, H. Kanatomi, Y. Demura, and I. Murase, *Bull. Chem. Soc. Jpn.*, **57**, 1003 (1984). b) M. Suzuki, A. Uehara, H. Oshio, K. Endo, M. Yanaga, S. Kida, and K. Saito, *Bull. Chem. Soc. Jpn.*, **60**, 3547 (1987). c) Y. Maeda, Y. Tanigawa, N. Matsumoto, H. Oshio, M. Suzuki, and Y. Takashima, *Bull. Chem. Soc. Jpn.*, **67**, 125 (1994).

3 a) S. Nakashima, Y. Masuda, I. Motoyama, and H. Sano, *Bull. Chem. Soc. Jpn.*, **60**, 1673 (1987). b) S. Nakashima, Y. Ueki, and H. Sakai, *J. Chem. Soc., Dalton Trans.*, **1995**, 513.

4 D. Lupu, D. Barb, G. Filoti, M. Morariu, and D. Tarina, *J. Inorg. Nucl. Chem.*, **34**, 2803 (1972).

5 a) T. Nakamoto, M. Katada, and H. Sano, *Chem. Lett.*, **1990**, 225. b) P. Poganiuch, S. Liu, G. C. Papaefthymiou, and S. J. Lippard, *J. Am. Chem. Soc.*, **113**, 4645 (1991). c) T. Nakamoto, M. Hanaya, M. Katada, K. Endo, S. Kitagawa, and H. Sano, *Inorg. Chem.*, **36**, 4347 (1997).

6 R. D. Cannon, U. A. Jayasooriya, R. P. White, and S. K. ArapKoske, *Specrochim. Acta, Part A*, **49A**, 1787 (1993).

7 a) S. E. Woehler, R. J. Wittebort, S. M. Oh, D. N. Hendrickson, D. Inniss, and C. E. Strouse, *J. Am. Chem. Soc.*, **108**, 2938 (1986). b) S. E. Woehler, R. J. Wittebort, S. M. Oh, T. Kambara, D. N. Hendrickson, D. Inniss, and C. E. Strouse, *J. Am. Chem. Soc.*, **109**, 1063 (1987). c) H. G. Jang, S. J. Geib, Y. Kaneko, M. Nakano, M. Sorai, A. L. Rheingold, B. Montez, and D. N. Hendrickson, *J. Am. Chem. Soc.*, **111**, 173 (1989). d) H. G. Jang, K. Kaji, M. Sorai, R. J. Wittebort, S. J. Geib, A. L. Rheingold, and D. N. Hendrickson, *Inorg. Chem.*, **29**, 3547 (1990). e) H. G. Jang, R. J. Wittebort, M. Sorai, Y. Kaneko, M. Nakano, and D. N. Hendrickson, *Inorg. Chem.*, **31**, 2265 (1992).

8 a) T. Kambara, D. N. Hendrickson, M. Sorai, and S. M. Oh, *J. Chem. Phys.*, **85**, 2895 (1986). b) S. M. Oh, S. R. Wilson, D. N. Hendrickson, S. E. Woehler, R. J. Wittebort, D. Inniss, and C. E. Strouse, *J. Am. Chem. Soc.*, **109**, 1073 (1987). c) S. M. Oh, D. N. Hendrickson, K. L. Hassett, and R. E. Davis, *J. Am. Chem. Soc.*, **107**, 8009 (1985).

9 T. Sato, F. Ambe, K. Endo, M. Katada, H. Maeda, T. Nakamoto, and H. Sano, *J. Am. Chem. Soc.*, **118**, 3450 (1996).

10 Y. Maeda, Y. Takashima, N. Matsumoto, and A. Ohyoshi, *J. Chem. Soc., Dalton Trans.*, **1986**, 1115.

11 a) C-C. Wu, H. G. Jang, A. L. Rheingold, P. Gütlich, and D. N. Hendrickson, *Inorg. Chem.*, **35**, 4137 (1996). b) C-C. Wu, S. A. Hunt, P. K. Gantzel, P. Gütlich, and D. N. Hendrickson, *Inorg. Chem.*, **36**, 4717 (1997).

12 R. Wu, M. Poyraz, F. E. Sowrey, C. E. Anson, S. Wocadlo, A. K. Powell, U. A. Jayasooriya, R. D. Cannon, T. Nakamoto, M. Katada, and H. Sano, *Inorg. Chem.*, **37**, 1913 (1998).

13 T. Manago, S. Hayami, H. Oshio, S. Osaki, H. Hasuyama, R. H. Herber, and Y. Maeda, *J. Chem. Soc., Dalton Trans.*, **1999**, 1001.

14 a) M. Sorai, K. Kaji, D. N. Hendrickson, and S. M. Oh, *J. Am. Chem. Soc.*, **108**, 702 (1986). b) M. Sorai, Y. Shiomi, D. N. Hendrickson, S. M. Oh, and T. Kambara, *Inorg. Chem.*, **26**, 223 (1987).

15 T. Nakamoto, M. Katada, and H. Sano, *Chem. Lett.*, **1991**, 1323.